MNRAS **000**, 1–8 (2018) Preprint 27 November 2018 Compiled using MNRAS LATEX style file v3.0

Physical properties of PHA 2014 JO_{25} from a worldwide observational campaign

Amadeo Aznar,[1⋆] J. de León,[2,3] M. Popescu,[2,3,4] M. Serra-Ricart,[2,3] P. Short, [5] P. Pravec, [6] O. Vaduvescu,[7,2] J. Licandro,[2,3] J. L. Ortiz,[8] A. Sota,[8] N. Morales,[8] V. Lorenzi,[9,2] B. Warner,[10] J. Oey,[11,12,13] R. Groom[12]

[1]*Observatorio Isaac Aznar, Grupo de Observatorios APT C/La Plana, 44, 13, 46530 Puçol, Valencia, Spain*
[2]*Instituto de Astrofísica de Canarias (IAC), C/Vía Láctea, s/n, 38205 La Laguna, Tenerife, Spain*
[3]*Departamento de Astrofísica, Universidad de La Laguna, 38205 La Laguna, Tenerife, Spain*
[4]*Astronomical Institute of the Romanian Academy, 5 Cuţitul de Argint, 040557 Bucharest, Romania*
[5]*Department of Physics and Astronomy, University of Sheffield, Sheffield, UK*
[6]*Astronomical Institute, Academy of Sciences of the Czech Republic Friova 1, CZ-25165 Ondrejov, Czech Republic*
[7]*Isaac Newton Group, Apt. de correos 321, E-38700, Santa Cruz de La Palma, Canary Islands*
[8]*Observatorio de Sierra Nevada, Instituto de Astrofísica de Andalucía (IAA), Consejo Superior de Investigaciones Científicas (CSIC) Apt 3004, 18080 Granada, Spain*
[9]*Fundación Galileo Galilei, INAF, Rambla José Ana Fernández Pérez, 7, E-38712 Breña Baja, La Palma, Spain*
[10]*Center for Solar System studies-Palmer-Divide Station, Landers, California, USA*
[11]*Blue Mountains Observatory, Leura, Australia*
[12]*Darling Range Observatory, Perth, Australia*
[13] *JBL Observatory, Bathurst, NSW, Australia*

Accepted XXX. Received YYY; in original form ZZZ

ABSTRACT

The study of minor planets is motivated both by fundamental science of Solar System origins (some of these bodies contain the most pristine materials from the early ages of the planetary nebula), and by practical reasons concerning space exploration and impact frequency with Earth. Among minor bodies, near-Earth asteroids (NEAs) are a particularly important group: these objects are nearby the Earth's orbit and they represent both resources and hazards to humans. This is the case of 2014 JO_{25}. The encounter of this potentially hazardous asteroid (PHA) with the Earth at 0.01175 au on April 19, 2017 was a good opportunity to study its properties through photometric and spectral analyses. The work we present here has been carried out thanks to a worldwide observational campaign that included time-series photometry and spectroscopy in the visible and near-infrared wavelengths. The optical images for photometric analysis were collected at different phase angles using small telescopes (< 0.5 meters) and medium telescopes (from 0.6 to 1.5 meters). Spectral analysis was performed by 2-4 meters telescopes. The light curve of 2014 JO_{25} indicates a synodic rotational period of 4.5286 ± 0.0004 hours. Although rotational period had been previously obtained by other authors, this work confirms it with a better accuracy. The obtained reflectance spectrum of this asteroid indicates that it belongs to the S-complex and its surface is most likely composed of a mixture of pyroxenes and olivine. From the comparison of its spectrum to those of meteorite samples, as well as from the wavelength position of the first absorption band (close to 0.9 μm), we suggest that this asteroid might contain a large fraction of low-calcium pyroxene and, tentatively, some amounts of metal.

Key words: techniques: photometric – techniques: spectroscopic – minor planets, asteroids: individual: 2014 JO_{25}

1 INTRODUCTION

The study of near Earth asteroids (NEAs) represents one of the most interesting topics in planetary science, as it could bring insights about the formation of minor bodies and the early stages

⋆ E-mail: aptog@aptog.com (AA)

of the Solar System. The close approach to the Earth of asteroid 2014 JO_{25} on April 19, 2017 was a good opportunity to increase our knowledge about potentially hazardous asteroids (PHAs). This target was discovered by the Catalina Sky Survey on May 5, 2014 (MPS 514080), passing at 0.01175 au from the Earth in what was considered as the closest approach of a large (600 m) asteroid after Toutatis in 2004.

Due to its small Earth minimum orbital intersection distance (MOID) of less than 0.05 au, and its large size, i.e., as of October 9, 2018, its absolute magnitude is listed as H=17.8[1] by the JPL Small-Body Database Browser (Giorgini et al. 1996), 2014 JO_{25} has been classified as a PHA that follows an Apollo-type orbit, highly eccentric and inclined (e=0.88; i=25.2°), and with a semi-major axis of 2.06 au, a perihelion distance q=0.24 au and an aphelion distance Q=3.90 au[2]. Radar observations were conducted by the Arecibo Observatory on April 19, 2017 with a resolution of 7.5 m/pix, and by Goldstone radar from April 16-21 (Naidu et al. 2017). The radar images show that 2014 JO_{25} has an irregular shape, suggesting two joined lobes with many concavities and convexities. Based on these observations, it was found that its size was larger than initially estimated (600 meters) assuming a spherical shape. Thanks to the radar observations, its maximum axis was set to roughly 1 km. According to observations done by the NEOWISE team (J. Masiero), 2014 JO_{25} has an optical albedo of about 0.25. This value is in agreement with the one estimated from the radar images (0.2), and also with the asteroid being classified as an S-type from the near-infrared spectrum obtained by J. Emery, L. McGraw and M. Lucas (University of Tennessee) and C. Thomas (Planetary Science Institute) using the SpeX instrument at the 3.0m NASA IRTF telescope. Both optical albedo value and near-infrared spectrum have not been published but are available at the CNEOS webpage [3]

During its 2017 flyby, 2014 JO_{25} became very interesting to the scientific community. As it happens with other NEAs, its close approach was a good opportunity to study in detail its physical properties (Müller et al. 2004, 2017; de León et al. 2013). Therefore, we carried out photometric and spectroscopic observations in a worldwide coordinated campaign between April 20 and May 17, 2017 in order to study this object. These observations as well as the data reduction are described in Section 2. Based on our obtained light curve data we analyze in Section 3 possible reasons for its rapidly changing light curve, among which its binary nature and a potential non-principal axis rotation (Pravec et al. 2005) are considered. The results of the spectroscopic observations are presented and analyzed in Section 4.

This work has been carried out in the frame of the European Near Earth Asteroid Research (EURONEAR)[4] and is the result on an international cooperation between observatories located in different continents and latitudes, such as Europe, Australia and Americas. Without this cooperation, this research would have been impossible due to the trajectory of 2014 JO_{25} (in both hemispheres) and its very fast fly-by.

2 OBSERVATIONS AND DATA REDUCTION

Asteroid 2014 JO_{25} was observed in 13 different nights, from April 20 to May 7, 2017. Nine observing facilities (public and private) were used to take CCD images in order to provide a wide coverage of the asteroid rotation: the 0.8m IAC80 telescope (Teide Observatory, Tenerife, Spain); the 1.5m T150 telescope (Sierra Nevada Observatory, Andalucía, Spain); the 0.8m T80 telescope (La Hita Observatory, Toledo, Spain); the 0.4m ASH2 telescope (San Pedro de Atacama Celestial Explorations Observatory - SPACEOBS, Chile); the 0.35m telescope (Isaac Aznar Observatory, Spain); the 0.35m telescope (Blue Mountains Observatory, Australia); the 0.32m telescope (JBL Observatory, Australia), the 0.30m telescope (Darling Range Observatory, Australia) and the 0.30m CS3-Palmer Divide Station Landers (USA). Details of the telescopes used and equipment specifications are presented in Table 1.

Due to the fast movement of the asteroid in the sky, mainly during the first nights after the asteroid closest approach to the Earth (April 17), we used short integration times. The integration time for each image was fixed taking into account the asteroid's apparent velocity and visual magnitude, with the aim of obtaining the optimum signal to noise. The minimum integration time was 5 seconds during April 20 for images captured by Palmer Divide Station CS3 and 10 seconds for images captured by Observatorio Isaac Aznar T35 telescope during the same night. The maximum integration time was 400 seconds for images acquired by the Observatorio de Sierra Nevada T150 telescope during May 17, when the asteroid reached an apparent visual magnitude m_V = 19.02. This maximum integration time was consistent with the maximum time recommended in order to avoid a smooth light curve (Pravec et al. 2000). The observing circumstances of each run are presented in Table 2. The asteroid proper motion, geometric distance, and phase angle were obtained from the Minor Planet Center[5], while latitude and longitude phase angle bisectors were extracted from the JPL HORIZON Web-Interface[6]. The Phase Angle Bisector (PAB) is the direction that points midway between the asteroid-Earth and asteroid-Sun directions as it would be seen by an observer located on the asteroid (Slivan et al. 2003).

All data was reduced using MPO *Canopus*[7] V10. Images were bias and flat-field corrected. In the case of images obtained with the Isaac Aznar Observatory T35, CS3-Palmer Divide Station Landers T30, Blue Mountains Observatory T35, and Darling Range Observatory T30 and T35 telescopes, dark frame correction was also included in the image calibration process.

Differential aperture photometry was obtained. The photometric reference catalog was MPOSC3, provided with MPO software. This catalog is a hybrid of the Sloan Digital Sky Survey (SDSS) and Carlsberg Meridian Catalog, and contains about 150-M type stars. Current version of this catalog includes, when available, SDSS *g*'*r*'*i*' magnitudes in addition to BVRI ones, and reports a photometric average error around 0.05 mag. Solar type comparison stars in the field were selected during differential photometry reduction. Although all observations were carried out using a clear filter in order to maximize the asteroid light flux signal, V magnitudes of comparison stars were selected to obtain the calibrated V magnitude of the asteroid. Light-travel time to Earth was considered to correct the time of each image. Finally, a Fourier analysis (Harris et al. 1989; Pravec et al. 1996) included in MPO *Canopus* was used to search for the rotation period of the asteroid that best fits

[1] https://ssd.jpl.nasa.gov/sbdb.cgi#top
[2] https://www.minorplanetcenter.net
[3] https://cneos.jpl.nasa.gov/news/news196.html
[4] http://www.euronear.org
[5] https://www.minorplanetcenter.net/
[6] https://ssd.jpl.nasa.gov/horizons.cgi
[7] http://www.minorplanetobserver.com/MPOSoftware/MPOCanopus.htm

Table 1. Instrumental setup used to obtain photometric data of 2014 JO_{25}. The information includes the name of the observatory and telescope used, geographical coordinates (latitude and longitude), telescope aperture (in meters), type of CCD, binning, plate scale and total number of images (N).

Observatory/Telescope	Latitude (° ' ")	Longitude (° ' ")	Aperture (m)	CCD type	Binning	Plate scale ("/pixel)	N
Isaac Aznar/T35	39 57 01 N	01 06 33 W	0.35	STL-1001E	1x1	1.44	1,310
CS3-Palmer Divide Station/T30	34 15 00 N	116 45 23 W	0.30	ML-1001E	1x1	1.72	1,135
Teide/ IAC80	28 17 56 N	16 30 35 W	0.80	SI-600	1x1	0.33	577
La Hita/T80	39 35 53 N	03 06 53 W	0.77	STX-16803	1x1	0.84	573
Darling Range/T30	31 52 53 S	116 10 12 E	0.30	ST8-XME	1x1	0.84	364
JBL Observatory/T32	33 23 48 S	149 29 32 E	0.32	STL-11000M	1x1	0.66	212
SPACEOBS/ASH2	22 57 15 S	68 10 45 W	0.40	STL-11000M	1x1	1.22	192
Blue Mountains/T35	33 42 22 S	150 20 30 E	0.35	Apogee U6-2048B	2x2	0.46	106
Sierra Nevada/T150	37 03 51 N	03 23 05 W	1.50	VersArray-2048B	2x2	0.46	71
						Total	4,540

Table 2. Observational details of the photometric measurements. We include the telescope and observatory, observing date, time span, number of images (N), asteroid proper motion, geocentric distance (Δ), phase angle (α), apparent visual magnitude (m_V), latitude phase angle bisector (PAB-LT), and longitude phase angle bisector (PAB-LN). Observations marked with an asterisk were used to derive the rotational period.

Telescope/Observatory	Date	Time span (hours)	N	Proper motion ("/min)	Δ (au)	α (°)	m_V	PAB-LT (°)	PAB-LN (°)
T35/Palmer Divide Station CS3	April 20	7.2	328	117.68-73.73	0.019	33.9	11.0	12.44	197.66
T35/Isaac Aznar	April 20	6.0	820	45.91-34.10	0.030	25.5	11.74	4.58	198.11
T35/Palmer Divide Station CS3	April 21	6.0	265	28.96-22.13	0.036	24.6	11.684	2.67	198.33
T35/Isaac Aznar*	April 21	5.5	318	16.30-12.54	0.049	23.8	12.76	-0.05	198.73
T80/La Hita*	April 21	4.5	401	14.33-13.22	0.050	23.9	12.80	-0.17	198.75
T35/Palmer Divide Station CS3	April 22	5.0	248	11.81-10.08	0.053	24.0	12.47	-0.89	198.90
IAC80/Teide*	April 22	2.0	283	7.54-7.18	0.068	24.3	13.53	-2.18	199.20
T35/Palmer Divide Station CS3	April 23	5.5	162	6.38-5.69	0.072	24.4	13.65	-2.48	199.29
T35/Isaac Aznar*	April 23	4.8	172	4.52-4.18	0.087	24.4	14.12	-3.44	199.59
T80/La Hita*	April 23	4.5	172	4.56-4.26	0.087	24.9	14.12	-3.44	199.59
T30/Darling Range	April 23	2.5	102	5.39-5.16	0.080	24.7	13.89	-3.00	199.43
T35/Palmer Divide Station CS3	April 24	3.5	132	3.87-3.62	0.093	25.1	13.96	-3.74	199.71
IAC80/Teide*	April 24	6.8	294	3.06-2.79	0.106	25.5	14.63	-4.30	199.95
T32/JBL Observatory	April 25	5.0	55	2.46-2.20	0.119	25.9	14.46	-4.68	200.15
T30/Darling Range	April 26	5.0	90	1.81-1.67	0.139	26.3	15.27	-5.21	200.46
T35/Blue Mountain	April 27	3.5	28	1.44-1.33	0.164	26.7	15.68	-5.71	200.82
T30/Darling Range	April 27	6.5	62	1.42-1.28	0.136	26.7	15.56	-5.58	200.72
T32/JBL Observatory	April 27	3.5	40	1.43-1.37	0.136	26.7	15.56	-5.58	200.72
T30/Darling Range	April 28	4.0	30	1.12-1.06	0.177	27.2	15.88	-5.95	201.02
T32/JBL Observatory	April 28	6.5	64	1.12-0.98	0.177	27.2	15.88	-5.95	201.02
T35/Blue Mountains	April 29	7.0	78	1.14-0.99	0.223	27.5	16.24	-6.33	201.39
T30/Darling Range	April 29	6.5	67	0.90-0.85	0.197	27.5	16.16	-6.25	201.30
T32/JBL Observatory	April 29	4.0	40	0.91-0.87	0.195	27.5	16.12	-6.21	201.27
T30/Darling Range	April 30	2.0	26	0.75-0.72	0.207	27.8	16.63	-6.73	201.83
T40/SPACEOBS	May 2	5.5	72	0.48-0.45	0.267	28.6	16.90	-7.03	202.20
T150/Sierra Nevada	May 3	4.3	44	0.43-0.42	0.283	28.8	16.91	-6.99	202.16
T40/SPACEOBS	May 3	6.0	74	0.42-0.40	0.303	28.8	17.10	-7.20	202.45
T40/SPACEOBS	May 4	6.0	46	0.37	0.307	29.0	17.30	-7.36	202.69
T150/Sierra Nevada	May 17	2.80	27	0.36	0.569	31.0	19.02	-8.71	205.57

the observations. The composed light curves for different nights are shown in Fig.1.

3 PHOTOMETRIC RESULTS

Several light curves of the asteroid were obtained during 13 nights from April 20 to May 17, 2017. The analysis of this photometric dataset is not trivial. The shape of the light curve is not the typical one with 2-maxima and 2-minima shown by most asteroids. As discussed in Section 1, 2014 JO_{25} presents a complex shape, formed by two lobes and with several concavities. In addition, during its close approach to the Earth (mainly from April 20 to 22) the geometry of the observations (in particular the aspect angle), and thus the shape of the observed light curve changed very rapidly (Zappala et al. 1990). Finally, changes in the phase angle bisector among data from different observatories, especially in latitude, imposed additional difficulties in the composition of the light curves (Harris et al. 2014). Taking all these factors into account we have composed the light curves for 2014 JO_{25} using data from similar ge-

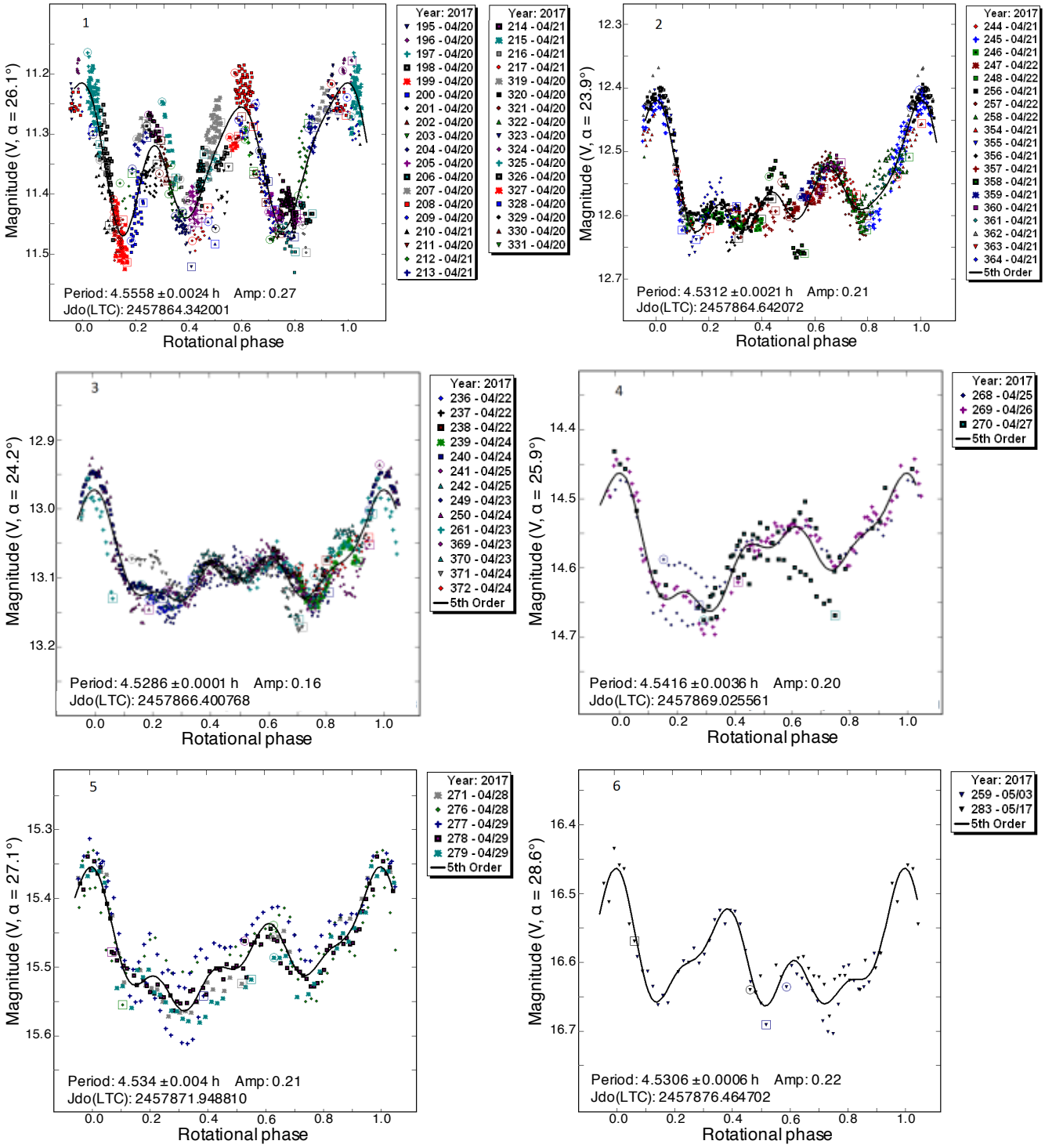

Figure 1. Light curve evolution sequence: 1) April 20 composed data set from Isaac Aznar Observatory and CS3 Palmer Divide Station ; 2) April 21 composed data set from Isaac Aznar Observatory, CS3 Palmer Divide Station and La Hita Observatory; 3) April 22-24 composed data set from Isaac Aznar Observatory, CS3 Palmer Divide Station, La Hita Observatory, and Teide Observatory; 4) April 25-27 composed dataset from JBL Observatory, Darling Range Observatory and Blue Mountain Observatory; 5) April 28-29 composed dataset from Darling Range Observatory; 6) May 3 and May 16 composed dataset from Observatorio Sierra Nevada. Each panel shows the computed rotational period using the corresponding dataset, as well as the amplitude of the light curve (Amp) and the Julian Date when the first dataset was obtained (JDo). Different symbols within each panel correspond to different observational sessions. Open symbols correspond to the first (circle) and the last (square) data point of each session.

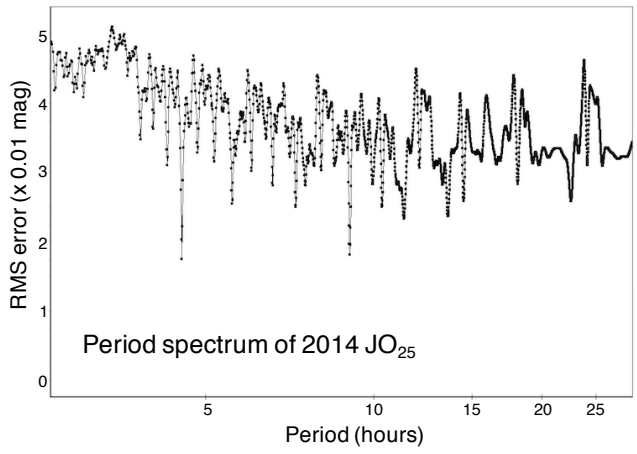

Figure 2. Periodogram analysis of the data obtained from April 21 to April 24 with the Teide IAC80, La Hita T80, and Isaac Aznar T35 telescopes using the Fourier analysis.

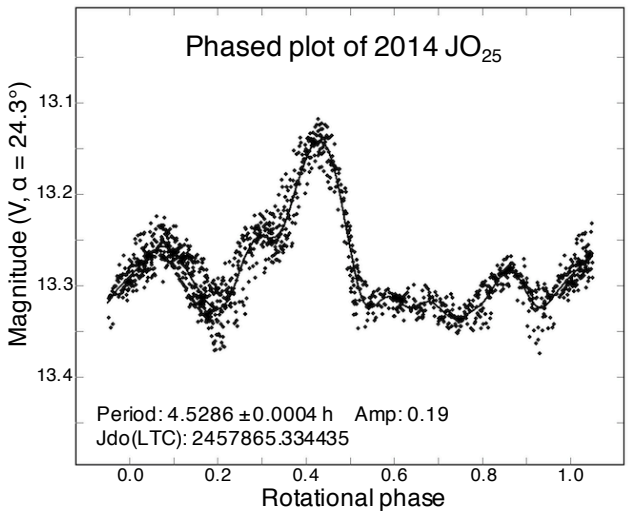

Figure 3. light curve using data obtained from T35 telescope (April 21, April 23), La Hita T80 (April 21, April 23) and IAC80/Teide (April 22, April 24).

The data have been phased using our best determined synodic period (P_{rot} = 4.5286 ± 0.0004 hours).

ographical coordinates obtained during restricted periods of time, in order to reduce the effect of the asteroid changing aspect.

To derive the rotation period we used a restricted dataset using the observations done with the Teide IAC80, La Hita T80, and Isaac Aznar T35 telescopes from April 21 to April 24 (marked with an asterisk in Table 2. The Fourier analysis provided a best fit with a synodic period of P_{rot} = 4.5286 ± 0.0004 hours (Fig. 2). The periodogram shows two possible rotation periods: the first one (4.5286 ± 0.0004 hours) is the one we adopted. This period provides the lower rms error. The second one is 9.056 hours which is double of the first one, and it is likely an alias. Our derived rotational period is similar that of 4.53 ± 0.02 hours obtained by Warner (2017) using data of the Palmer Divide Station CS3 alone and to that of 4.530 ± 0.002 obtained by Tan et al. (2018), but with a higher accuracy. The composed light curve shown in Fig. 3 presents a complex shape as expected, with a maximum amplitude of 0.19 magnitudes. The obtained rotational period is quite typical for NEAs in the given size range (Pravec & Harris 2000; Pravec et al. 2002). The amplitude is on the low side of the amplitude distribution for NEAs with periods of 4-5 hours. Therefore, 2014 JO$_{25}$ is either more spheroidal than typical for NEAs of similar sizes and rotation rates (which might suggest something about its origin), or we observed it at an aspect not very far from pole-on that lowered its amplitude. Considering the double-lobed shape of the asteroid from radar images, the second explanation is the most suitable. We calculated the light curve amplitude at zero phase angle using the expression A(0°) = A(α) / (1+$m\alpha$), where A is the amplitude and m is a slope parameter (Zappala et al. 1990), know to be 0.03 for S-type asteroids. With the corrected amplitude and assuming a simple triaxial body model with $a > b > c$ and that the object rotation is about the c axis, we estimated a lower limit for the $a/b > 1.11$.

In Fig. 1 we present the composite light curves obtained for different periods of time using P_{rot} = 4.5286 hours. The variations in the shape of the light curves previously reported by Warner (2017) is very obvious, in particular from April 20 to April 21, during the closest approach to the Earth of the asteroid. As explained above, these light curves variations are somehow expected due to the complex shape of 2014 JO$_{25}$ and the rapid variation of the aspect angle during its close approach.

Another alternative explanation for the observed change in the shape of the light curves every two or three days is the possible binary nature of 2014 JO$_{25}$ (Pravec et al. 2016). To study this, we used the iterative subtraction process described in Pravec et al. (2006). We applied it to a restricted set of high quality data with photometric errors less than 0.03 magnitudes and we found that the light curve appeared periodic on intervals with lengths of up to 2 days with no deviations from the mean light curve that would be caused by a satellite or a non-principal axis rotation of the asteroid. The apparent light curve changes over longer intervals were likely related to a changing viewing geometry of the complex-shaped asteroid observed close to the Earth. Therefore, the light curve variations seem to be caused by the signature of the shape of the asteroid, with large concavities, on the evolving illumination and viewing geometries. Further modeling using all published light curves and the radar observations could be used to retrieve a good shape model and derive better rotational properties of this asteroid.

4 SPECTRAL OBSERVATIONS

Spectral observations were done with the 2.54m Isaac Newton Telescope (INT) and the 3.58m Telescopio Nazionale Galileo (TNG), both located at the El Roque de los Muchachos Observatory, in La Palma (Canary Islands, Spain). The observations were performed on the night of May 3, 2017 with the TNG and May 4, 2017 with the INT. During both nights the humidity was high (≈ 80%) and the seeing was variable (between 1-2"). The observational details are shown in Table 3.

Visible INT spectra were obtained with the IDS (Intermediate Dispersion Spectrograph) using the R150 grism diffraction element and the EEV10 CCD camera. A slit of 1.5" width (about 4 pixels) was set as a trade off between the variable seeing and resolution. This configuration allows to cover the spectral interval ∼ 0.4-0.9 μm with a dispersion of 0.4 nm/pixel. All observations were performed by orienting the slit at parallactic angle, to minimize the effects of atmospheric differential refraction, and the tracking of

the telescope was set at the asteroid's proper motion. We obtained 5 spectra of 1200 seconds of exposure time each. We also observed a total of three G2V solar analog stars in the same airmass range as that of the object: Landolt SA 102-1081 (Landolt 1992), HD 106042, and HD106061.

Images were bias and flat-field corrected using standard procedures. The two-dimensional spectra were extracted, sky background subtracted, and collapsed to one dimension. All these steps were done using IRAF[8]. Each image was visually inspected to avoid the contamination with background stars or movement of the object out of the slit. The wavelength calibration was performed using emission lines from Cu-Ar and Cu-Ne lamps. The asteroid spectrum was divided by the individual spectrum of each solar analog. The resulting reflectance spectra presented no variations when compared to each other and so, they were all averaged and normalized to unity at 0.55 μm.

Near-infrared TNG spectra were obtained with the low resolution mode of NICS (Near Infrared Camera Spectrograph), based on a HgCdTe Hawaii 1024x1024 array. We used the Amici prism disperser that provides a complete 0.9-2.4 μm spectrum, with a 1.5" slit width. As in the case of visible observations, the slit was oriented in the parallactic angle and the tracking was set at the asteroid's proper motion. The acquisition followed the typical nodding procedure: we obtained an image of 90 seconds in one position (position *A*) of the slit and then we offset the telescope by 10" in the spatial direction to obtain another image (position *B*). This process was repeated, and a total of 11 *ABBA* cycles were acquired. To correct for telluric absorptions and to get the reflectance spectra of the asteroid, two G2V solar analog stars were observed at the same airmass as that of the object: P041C (Colina & Bohlin 1997) and Landolt SA102-1081.

Images were flat-field corrected and *AB* pairs were obtained by subtracting consecutive *A* and *B* images. Details on the subtraction process can be found in Licandro et al. (2001). The one-dimensional spectrum was finally extracted from each *AB* pair. Wavelength calibration of the individual spectra of the asteroid was performed simultaneously to the division by the spectra of the solar analog stars, using a specific program developed by the telescope staff and available upon request. As in the case of the visible observations, we verified that there were no significant variations among the resulting reflectance spectra and we averaged them to obtain the final near-infrared spectrum, normalized to unity at 1.6 μm. We merged the visible and the near-infrared spectra (Fig. 4) using the common wavelength region at 0.80-0.85 μm. Our near-infrared spectrum is practically identical to the one reported by CNEOS[9] and obtained with the 3.0m IRTF telescope (Hawaii).

For the taxonomic classification we used M4AST curve matching tools (Popescu et al. 2012) and SMASS - MIT[10] website. According to these tools, the asteroid belongs to the S-complex and more specifically, it is an intermediate type between an Sr- and a Q-type: the visible part of the spectrum is closer to a Q-type while the near-infrared part resembles that of an Sr-type. This classification is in agreement with the asteroid belonging to the S/Q complex as derived recently by Petropoulou et al. (2018) from visible spectra. However, the wavelength position of the first absorption band is lower than expected for an S/Q-type asteroid.

As a member of the S-complex, the spectrum of 2014 JO_{25} shows the two strong absorption features centred around 1 and 2 μm associated to silicates (mainly olivine and pyroxene). Using the M4AST tool, we compared the visible and near-infrared spectrum of this object to the more than 2,500 reflectance spectra of meteorites available in the RELAB public database (Pieters & Hiroi 2004). We found that the best 3 matches correspond to samples of L6 ordinary chondrites: Jackalsfontein (sample ID: MB-CMP-012-L); Tourinnes-la-Grosse (sample ID: MR-MJG-063); and Zavid (sample ID: MR-MJG-063). We have plot the spectrum of Jackalsfontein L6 meteorite as a red line in Fig. 4. The value of absolute reflectance of this meteorite at 0.55 μm, which is commonly assumed to be roughly comparable to asteroidal geometric albedo, is 0.289, in good agreement with the average albedo of S-complex asteroids (Mainzer et al. 2011), and with the optical albedo of 2014 JO_{25} obtained from NEOWISE observations (0.25). Actually, the results are very consistent: from the first 25 best meteorite matches provided by the M4AST tool, 18 correspond to L chondrites, and from these, 12 are L6 chondrites. Despite this good agreement, the minimum of the first absorption band for 2014 JO_{25} is still located at slightly lower wavelengths compared to that of the L chondrites. We discuss about this point in the next paragraph.

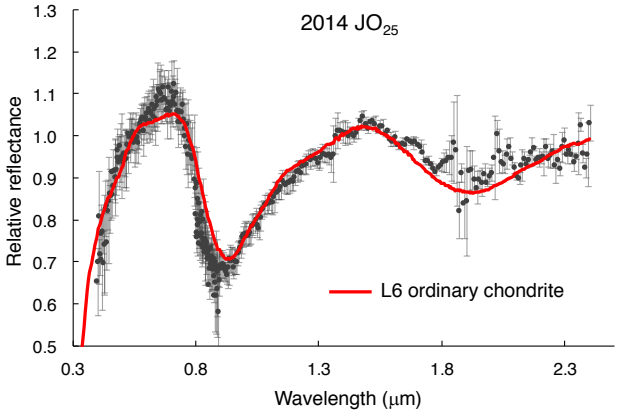

Figure 4. Visible and near-infrared spectra of 2014 JO_{25} obtained with the INT and the TNG telescopes, respectively. The overall spectrum is normalized to unity at 0.55 μm. The error bars correspond to 1σ deviation of the average. The spectrum of 2014 JO_{25} best matches the spectra of L6 ordinary chondrites (red line).

Following the methods first described by Cloutis et al. (1986) and Gaffey et al. (1993), we can compute several spectral parameters on the spectrum of 2014 JO_{25} (wavelength positions of the absorption bands, band area ratio, etc) which are related to its composition and in this way, we can determine mafic mineral abundances on its surface, among other properties. We computed the band minima (BImin and BIImin), the band centres (BIC and BIIC, once the continuum has been removed) and the band area ratio (BAR) following the procedures summarized in Reddy et al. (2015) and references therein. This method was mainly developed to study main belt asteroids and so, we have to apply a temperature correction to account for the higher surface temperature of a near-Earth asteroid. We computed the temperature corrections for the Band II centre (ΔBIIC) and for the BAR (ΔBAR) parameter following Sanchez et al. (2012). We derived the olivine/pyroxene ratio (Ol/Ol+Px), and the iron content in the olivine and the pyroxene, expressed as the molar percentage of fayalite (Fa, Fe_2SiO_4) and ferrosilite (Fs, $FeSiO_3$), respecitvely, using the relations described in Dunn et al. (2010). The results are summarized in Table 4.

[8] Image Reduction and Analysis Facility, Tody 1993
[9] https://cneos.jpl.nasa.gov/news/news196.html
[10] http://smass.mit.edu/busdemeoclass.html

Table 3. Observational details for 2014 JO$_{25}$ spectral data. Information includes the telescope used, date of observation, UT starting time, exposure time, average airmass, apparent visual magnitude (m$_V$), phase angle (α), and heliocentric distance (r).

Telescope	Date	UT	Exp. time (secs)	Airmass	m$_V$	α (°)	r (au)
TNG	2017-05-03	22:32	11 x 360	1.360-1.500	17.1	29	1.263
INT	2017-05-04	22:12	5 x 1200	1.365-1.623	17.3	28.8	1.248

Table 4. Computed band parameters and derived modal mineralogy.

Parameter	Computed value
BImin	0.920 ± 0.016 μm
BIImin	1.900 ± 0.042 μm
BIC	0.915 ± 0.019 μm
BIIC	1.894 ± 0.039 μm
ΔBIIC	0.013 μm
BAR	0.421 ± 0.120
ΔBAR	0.053
Ol/Ol+Px	0.602 ± 0.033
Fa	14.5 ± 5.1 mol %
Fs	13.4 ± 3.6 mol %

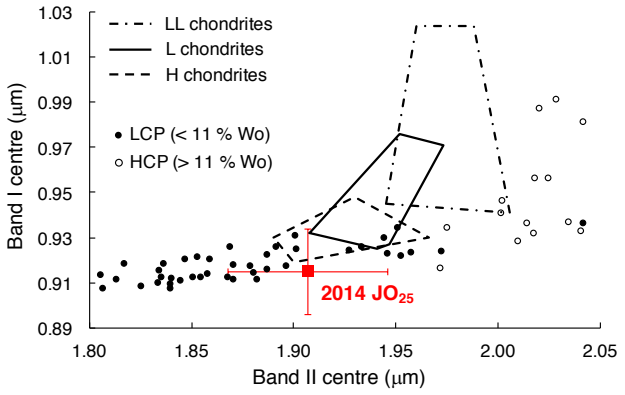

Figure 5. Band II centre vs. Band I centre for a sample of low calcium (solid symbols) and high calcium (open symbols) pyroxenes, from Cloutis & Gaffey (1991). The regions outlined by the LL, L, and H ordinary chondrites are also indicated. The red square shows the position of 2014 JO$_{25}$.

Fig. 5 shows the wavelength position of the Band I and Band II centres (Cloutis & Gaffey 1991) of a sample of low calcium (solid symbols, < 11% Wo) and high calcium (open symbols, > 11% Wo) pyroxenes (LCP and HCP, respectively). We also show in Fig. 5 the regions occupied by LL, L, and H ordinary chondrites. As it can be seen, 2014 JO$_{25}$ lies outside the regions defined by the ordinary chondrites, mainly due to the lower position of its Band I centre, but it is within the region occupied by the LCPs (solid symbols). Furthermore, the chemical analysis available for the sample of L6 meteorite Tourinnes-la-Grosse (second best match) indicate a low calcium content of the pyroxene in this meteorite (< 4 % Wo). In addition, two of the three best meteorite matches to the spectrum of 2014 JO$_{25}$ correspond to L6 chondrites that present some amount of metal, either in the form of "rust" or as a small molar percentage in a mixture. According to Cloutis et al. (1990) and Cloutis et al. (2015), the addition of metal in olivine/metal and pyroxene/metal mixtures produces a shift to shorter wavelengths of the position of the 1 μm absorption band.

5 CONCLUSIONS

The near-Earth asteroid 2014 JO$_{25}$ close encounter in 2017 with the Earth was a good opportunity to coordinate efforts from different observatories and maximize the scientific outcome of this close approach. The brightness of the target allowed the contribution of small telescopes, taking into account the asteroid path from North to South, involving facilities from both hemispheres. Thanks to such cooperation it has been possible to make a deep photometric analysis in order to derive some physical properties of this target. In addition, spectroscopic observations allowed to derive detailed mineralogical information on the surface of this potentially hazardous object.

After collecting 4,540 photometric data grouped in 29 work sessions we derived a rotational period for 2014 JO$_{25}$ of P_{rot} = 4.5286 ± 0.0004 hours using a Fourier periodogram analysis. From the analysis of the maximum amplitude of the asteroid light curve and its evolution with phase angle, we conclude that 2014 JO$_{25}$ is not an extremely elongated object, with a maximum amplitude of 0.19 at a phase angle α = 24.3°, equal to an amplitude of 0.14 at phase angle α = 0° (Zappala et al. 1990). Assuming a simple triaxial body model with $a > b > c$ and that the object's rotation is about the c axis we determine a lower limit of $a/b > 1.11$.

Although we have detected variations in the shape of the asteroid light curves (mainly photometric data drops in some sections), we discard the presence of a satellite. This conclusion is supported by radar images obtained from the Arecibo Observatory and Goldstone radar (Naidu et al. 2017), which show that 2014 JO$_{25}$ is an irregular object, consisting of two components connected by a narrow neck, presenting concavities, flat regions, and boulders. Furthermore, the analysis performed on its rotation period allowed us to discard a tumbler nature for this target. We conclude that the light curve variations are therefore caused by the complex shape of the asteroid and the rapid variations of the observing geometry during its close approach to the Earth.

From spectral observations, we derived that this object belongs to the S-complex. Best meteorite matches based on its visible and near-infrared spectrum correspond to L6 ordinary chondrites. The fact that the position of the absorption band around 1μm is located at shorter wavelengths compared to what is found for S-type asteroids and, in general, ordinary chondrites, can be explained by a large fraction of low-calcium pyroxene (LCP), or, tentatively, by some amounts of metal.

The next encounter with the Earth of 2014 JO$_{25}$ will take place in April 2020[11], when the asteroid will reach an apparent visual magnitude of m$_V$ = 16.2 at a distance of 0.16 au. That encounter will be another good opportunity to improve the photometric analysis. Furthermore, new data could be collected under a latitude/longitude phase angle bisector around -1 and 244 degrees receptivity[12], contributing to generate a 3D model.

[11] http://www.minorplanetcenter.net/iau/MPEph/MPEph.html
[12] https://ssd.jpl.nasa.gov/sbdb.cgi#top

6 ACKNOWLEDGEMENTS

J. Licandro (JL), M. Serra-Ricart (MSR), O. Vaduvescu (OV), M. Popescu (MP), and J. de León (JdL) acknowledge support from the AYA2015-67772-R project (MINECO, Spain). JdL also acknowledges support from from MINECO under the 2015 Severo Ochoa Program SEV-2015-0548. The Isaac Newton Telescope and its service mode are operated on the island of La Palma by the Isaac Newton Group of Telescopes in the Spanish Observatorio del Roque de los Muchachos of the Instituto de Astrofísica de Canarias. The work of MP was also been supported by a grant of the Romanian National Authority for Scientific Research - UEFISCDI, project number PN-II-RU-TE-2014-4-2199. The research leading to these results has received funding from the European Union's Horizon 2020 Research and Innovation Programme, under Grant Agreement No. 687378. We thank E. Molinari for allocation of Director's Discretionary Time at the Telescopio Nazionale Galileo. The work by P. Pravec was supported by the Grant Agency of the Czech Republic, Grant 17-00774S. Observations at CS3 and continued support of the asteroid lightcurve database (LCDB; Warner et al., 2009) are supported by NASA grant 80NSSC18K0851.This paper is partially based on data taken at the 0.77m La Hita telescope, which is jointly operated by the Instituto de Astrofísica de Andalucia-CSIC and Astrohita. Blue Mountains Observatory is supported by the 2015 Shoemaker NEO grant.

REFERENCES

Cloutis E. A., Gaffey M. J., 1991, J. Geophys. Res., 96, 22
Cloutis E. A., Gaffey M. J., Jackowski T. L., Reed K. L., 1986, J. Geophys. Res., 91, 11
Cloutis E. A., Gaffey M. J., Smith D. G. W., Lambert R. S. J., 1990, J. Geophys. Res., 95
Cloutis E. A., et al., 2015, Icarus, 252, 39
Dunn T. L., McCoy T. J., Sunshine J. M., McSween H. Y., 2010, Icarus, 208, 789
Gaffey M. J., Burbine T. H., Piatek J. L., Reed K. L., Chaky D. A., Bell J. F., Brown R. H., 1993, Icarus, 106, 573
Giorgini J. D., et al., 1996, in AAS/Division for Planetary Sciences Meeting Abstracts #28. p. 1158
Harris A. W., et al., 1989, Icarus, 77, 171
Harris A. W., et al., 2014, Icarus, 235, 55
Licandro J., Oliva E., Di Martino M., 2001, A&A, 373, L29
Mainzer A., et al., 2011, ApJ, 741, 90
Müller T. G., Sterzik M. F., Schütz O., Pravec P., Siebenmorgen R., 2004, A&A, 424, 1075
Müller T. G., et al., 2017, A&A, 598, A63
Naidu S., et al., 2017, AGU Fall Meeting Abstracts,
Petropoulou V., Lazzarin M., Bertini I., Ochner P., La Forgia F., Siviero A., Ferri F., Naletto G., 2018, Planet. Space Sci., 158, 63
Pieters C. M., Hiroi T., 2004, in Mackwell S., Stansbery E., eds, Lunar and Planetary Science Conference Vol. 35, Lunar and Planetary Science Conference.
Popescu M., Birlan M., Nedelcu D. A., 2012, A&A, 544, A130
Pravec P., Harris A. W., 2000, Icarus, 148, 12
Pravec P., Šarounová L., Wolf M., 1996, Icarus, 124, 471
Pravec P., Hergenrother C., Whiteley R., Šarounová L., Kušnirák P., Wolf M., 2000, Icarus, 147, 477
Pravec P., Harris A. W., Michalowski T., 2002, in Bottke Jr. W. F., Cellino A., Paolicchi P., Binzel R. P., eds, Asteroids III. pp 113–122
Pravec P., et al., 2005, Icarus, 173, 108
Pravec P., et al., 2006, Icarus, 181, 63
Pravec P., et al., 2016, Icarus, 267, 267
Reddy V., Dunn T. L., Thomas C. A., Moskovitz N. A., Burbine T. H., 2015, in Michel P., DeMeo F. E., Bottke W. F., eds, Asteroids IV. pp 43–63, doi:10.2458/azu_uapress_9780816532131-ch003
Sanchez J. A., Reddy V., Nathues A., Cloutis E. A., Mann P., Hiesinger H., 2012, Icarus, 220, 36
Slivan S. M., Bowsher E. C., Chang B. W., 2003, Minor Planet Bulletin, 30, 29
Tan H., Yeh T., Li B., Gao X., 2018, Minor Planet Bulletin, 45, 57
Warner B. D., 2017, Minor Planet Bulletin, 44, 327
Zappala V., Cellino A., Barucci A. M., Fulchignoni M., Lupishko D. F., 1990, A&A, 231, 548
de León J., et al., 2013, A&A, 555, L2

This paper has been typeset from a TEX/LATEX file prepared by the author.